

1 **Large ensemble simulation for investigating predictability of precursor**
2 **vortices of Typhoon Faxai in 2019 with a 14-km mesh global nonhydrostatic**
3 **atmospheric model**

4 **Y. Yamada¹, T. Miyakawa², M. Nakano¹, C. Kodama¹, A. Wada³, T. Nasuno¹, Y. Chen², A.**
5 **Yamazaki¹, H. Yashiro⁴, M. Satoh²**

6 ¹Japan Agency for Marine-Earth Science and Technology.

7 ²Atmosphere and Ocean Research Institute, the University of Tokyo.

8 ³Meteorological Research Institutes, Japan Meteorological Agency.

9 ⁴National Institute for Environmental Studies.

10 Corresponding author: Yohei Yamada (yoheiy@jamstec.go.jp)

11 **Key Points:**

- 12 • A 1600-member ensemble simulation for Typhoon Faxai (2019) was performed using a
13 14-km mesh nonhydrostatic atmospheric model.
- 14 • The model successfully predicts the risk of Faxai's landfall in Japan two weeks in
15 advance.
- 16 • Reproducibilities of the precursor vortex and upper-tropospheric trough yield good
17 prediction of the formation and track of Faxai.
- 18

19 **Abstract**

20 Typhoon Faxai hit Japan in 2019 and severely damaged the Tokyo metropolitan area. To mitigate
21 such damages, a good track forecast is necessary even before the typhoon formation. To investigate
22 the predictability of the genesis and movement of a precursor vortex and its relationship with the
23 synoptic-scale flow, 1600-member ensemble simulations of Typhoon Faxai were performed using
24 a 14-km mesh global nonhydrostatic atmospheric model, which started from 16 different initial
25 days (i.e., 1600 members in total).

26 The results show that the model could predict an enhanced risk of a Faxai-like vortex heading
27 toward Japan two weeks before landfall, which was up to 70%. The reason for the enhancement
28 was a rapid increase in the members reproducing a precursor vortex from 15 to 12 days before
29 landfall in Japan. In addition, the upper-tropospheric trough played an essential role in the track
30 simulation of Faxai.

31

32 **Plain Language Summary**

33 Tropical cyclones severely damage coastal regions yearly. Typhoon Faxai hit Japan in 2019 and
34 severely damaged buildings, power grids, and cell phone networks in the Tokyo metropolitan area.
35 To mitigate such damages, better track forecast is necessary even from the timing before typhoon
36 formation. A large ensemble member (1600-member) and high-resolution (14-km) simulation was
37 performed to investigate the genesis and movement of the precursor vortex of Faxai in 2019 and
38 its relationship with the synoptic-scale environmental flow using a global nonhydrostatic
39 atmospheric model on the Supercomputer Fugaku.

40 The results show the model could predict an enhanced risk of a Faxai-like vortex heading toward
41 Japan two weeks before landfall. A reason for the enhancement was a rapid increase in the
42 members reproducing a precursor vortex from 15 to 12 days before landfall in Japan. In addition,
43 the upper-tropospheric trough played an essential role in the movement of the Faxai-like vortex.

44

45 **1 Introduction**

46 A tropical depression developed into a tropical cyclone (TC) named Faxai at 18 UTC on
47 September 4, 2019, at 18.6°N, 156.7°E, according to the Regional Specialized Meteorological
48 Center-Tokyo best track (RSMCBT). Faxai moved northwestward and reached a central pressure
49 of 955 hPa at 18 UTC on September 7. Faxai made landfall in the Tokyo metropolitan area of
50 Japan at 17 UTC on September 8. The relatively small TC caused very strong winds, particularly
51 in the metropolitan area, tremendously damaging buildings, power grids, and cell phone networks
52 (Japan Meteorological Agency, 2020; Miyamoto et al., 2022; Fudeyasu et al., 2022). A remarkable
53 feature of Faxai was that there were only approximately four days from the genesis to the landfall
54 (Fudeyasu et al., 2022).

55 To mitigate disasters associated with TCs, predicting a long lead time (LT) is necessary,
56 which requires good forecasts for TC formation and track, as well as precursor vortices. Nakano
57 et al. (2015) demonstrated that TC formation can be predicted two weeks in advance. However,
58 the track forecast after TC formation has not been investigated. In addition, although operational
59 numerical weather forecast models improve TC track forecasts, challenges such as enhanced use
60 of ensemble remain (Yamaguchi et al., 2017).

61 A TC track is largely controlled by a synoptic-scale flow (Chan, 2017; Ito et al., 2020).
62 Regarding the influence of synoptic-scale flow, Fudeyasu et al. (2022) mentioned that the upper-
63 tropospheric cold low (UTCL) approached a precursor vortex of Faxai. Wei et al. (2016) showed
64 that UTCLs can affect a TC track, depending on their relative distance and orientation. TCs in a
65 UTCL's southern half are more likely to intensify, whereas those in the northern half are more
66 likely to weaken; also, TCs in a UTCL's northeastern quadrant tend to weaken more slowly than
67 those in the western North Pacific climatology (Wei et al., 2016; Wada et al., 2022). By performing

68 ensemble simulations from different initial times, Wada et al. (2022) noted that variations in
69 atmospheric initial conditions yield variations in the effect of cut-off lows on TC track simulations.

70 Previous studies have suggested that ensemble simulations improve TC track forecasts
71 (Nakano et al., 2017; Magnusson et al., 2019). In addition, the use of high-resolution global models
72 in which convective storms are explicitly resolved further improves TC track forecasts (Nakano et
73 al., 2017; Yamada et al., 2016). To the best of our knowledge, large-number ensemble experiments
74 (e.g., ensemble size >100 from each initial time) using such high-resolution models have not been
75 performed, except by Nakano et al. (2022).

76 The Fugaku, a recently developed pre-exascale supercomputer in Japan, opens the door to
77 examine the predictability of TC tracks, even before its formation. In this study, we demonstrate
78 the effectiveness of large-member ensemble experiments with horizontal high-resolution in
79 predicting the occurrence of disasters due to the landfall of Faxai in Japan and then clarify the
80 predictability of the genesis and movement of the precursor vortices of Faxai and their
81 relationships with synoptic-scale flows.

82

83 **2 Experiments and data**

84 2.1 1600-member ensemble simulation for Faxai

85 2.1.1 Experimental setting

86 We performed high-resolution large ensemble simulations for Faxai with 1600 ensemble
87 members. The Nonhydrostatic ICosahedral Atmospheric Model (NICAM) (Tomita & Satoh, 2004;
88 Satoh et al., 2008, 2014) was used for the simulations with a 14-km horizontal mesh. The
89 configuration of the model was almost the same as that of Kodama et al. (2021). The aerosol effect

90 was not considered; using a slab ocean model with a 15-m depth, sea surface temperature (SST)
91 was calculated and nudged toward National Oceanic and Atmospheric Administration daily
92 optimum interpolation SST Version 2.1 (Huang et al., 2020) with a relaxation time of one week.
93 The atmospheric initial conditions were developed from NICAM-Local Ensemble Transform
94 Kalman Filter (LETKF) Japan Aerospace Exploration Agency (JAXA) Research Analysis
95 (NEXRA) (Kotsuki et al., 2019) dataset. The number of ensemble members in NEXRA was 100
96 every 6 h with a 1.25° horizontal resolution. We used all the 100 members of NEXRA at 18 UTC
97 each day from August 20 to September 4, 2019 (16 days). Thus, a 1600-member ensemble
98 simulation was performed to investigate the predictability of Faxai.

99 Faxai traversed Tokyo Bay at 18 UTC on September 8, 2019, referred to as the approaching
100 time in this study. An LT was defined with reference to the approaching time, and the 1600-
101 member ensemble simulation covered LTs from “LT04” (starting from September 4) to “LT19”
102 (starting from August 20), with 100-member runs for each LT.

103

104 2.1.2 Extracting Faxai-like vortex

105 To detect vortices like Faxai in our ensemble simulation, we employed a TC tracking
106 method modified from Nakano et al. (2015), which is described in Supporting Information Text
107 S1. In this study, we analyzed not only TC but also tropical depressions. Next, we selected Faxai-
108 like vortices from extracted tracks. We regard a vortex traversing within a 1000-km radius from
109 the genesis location of the real Faxai within 5 days before and after its genesis time (criterion B)
110 as a Faxai-like vortex. In addition, we extracted vortices approaching Japan from Faxai-like
111 vortices, which traversed within a 1000-km radius from Tokyo Bay within 5 days before and after

112 the time when the real Faxai existed over Tokyo Bay (criterion A). We classified Faxai-like
113 vortices into two types of vortices: type-AB vortex (satisfying both criteria A and B) and type-B
114 vortex (satisfying only criteria B). Supporting Information Text S2 provides more details, and
115 Supporting Information Fig. S1 shows the samples of tracks for type-AB and type-B vortices. In
116 this study, vortices were classified and named based on some condition. The names of the
117 classified vortices are listed in Supporting Information Table S1.

118 2.2 NICAM climatology ensemble simulation

119 A global atmospheric model predicts a different mean state from the analysis, as the
120 forecast time becomes longer (Vitart, 2014). For instance, Roberts et al. (2020) showed that
121 NICAM overestimated TC using a diagram. To clarify that our Faxai ensemble simulation results
122 are not given by such overestimation in NICAM, the results need to be compared with NICAM's
123 model climatology.

124 2.2.1 Experimental setting

125 To derive NICAM's model climatology, 64-member ensemble simulations were performed
126 from 2009 to 2019 with a time-slice framework (Kinter et al., 2013). These simulations started
127 from August 20, except for 2015. In 2015, the initial time was used as August 19 because of
128 numerical instability. The simulations were performed until September 30 (approximately 40
129 days). The atmospheric initial conditions were created from the Atmospheric General Circulation
130 Model for the Earth Simulator–LETKF experimental ensemble reanalysis 2 (ALERA2; Enomoto
131 et al., 2013). The experimental setting was the same as that in the 1600-member ensemble
132 simulation for Faxai.

134 2.2.2 Extracting Faxai-like vortices

135 Vortex tracks were detected in the NICAM climatology ensemble simulation using the
136 almost same method as in the 1600-member ensemble simulation for Faxai (Supporting
137 Information Text S1). Because Faxai 2019 was generated in early September 2019, we assumed
138 vortices generated in early September 2019 in the climatology ensemble simulations as Faxai-like
139 vortices. The NICAM climatology ensemble simulations were run for a specific initial date each
140 year, unlike the 1600-member ensemble simulation for Faxai. Although Faxai-like vortices were
141 selected from the track data using the same method as in the 1600-member ensemble simulation
142 for Faxai (Supporting Information Text S2), the genesis time was shifted from September 1 to 20
143 for each ensemble member. To distinguish type-AB vortex from type-B vortex, criterion A was
144 applied to the Faxai-like vortices with the time lag between the genesis and approaching times
145 fixed to 4 days. The averages of the numbers were used as the climatology of the genesis
146 probability of type-AB and type-B vortices in early September.

147

148 2.3 Data

149 The RSMCBT and early-stage Dvorak analysis data (EDA) provided by the Japan
150 Meteorological Agency (JMA; Kishimoto, 2008) were used as the reference locations of Faxai.
151 Because, In the RSMCBT, the real Faxai was generated at 18 UTC on September 4, 2019, we
152 called the real precursor vortex of Faxai Pre-Faxai. The location of Pre-Faxai before the EDA was
153 extracted from a reanalysis. The fifth-generation European Centre for Medium-Range Weather
154 Forecasts (ECMWF) atmospheric reanalysis (ERA5; Hersbach, 2020) was employed in this study.

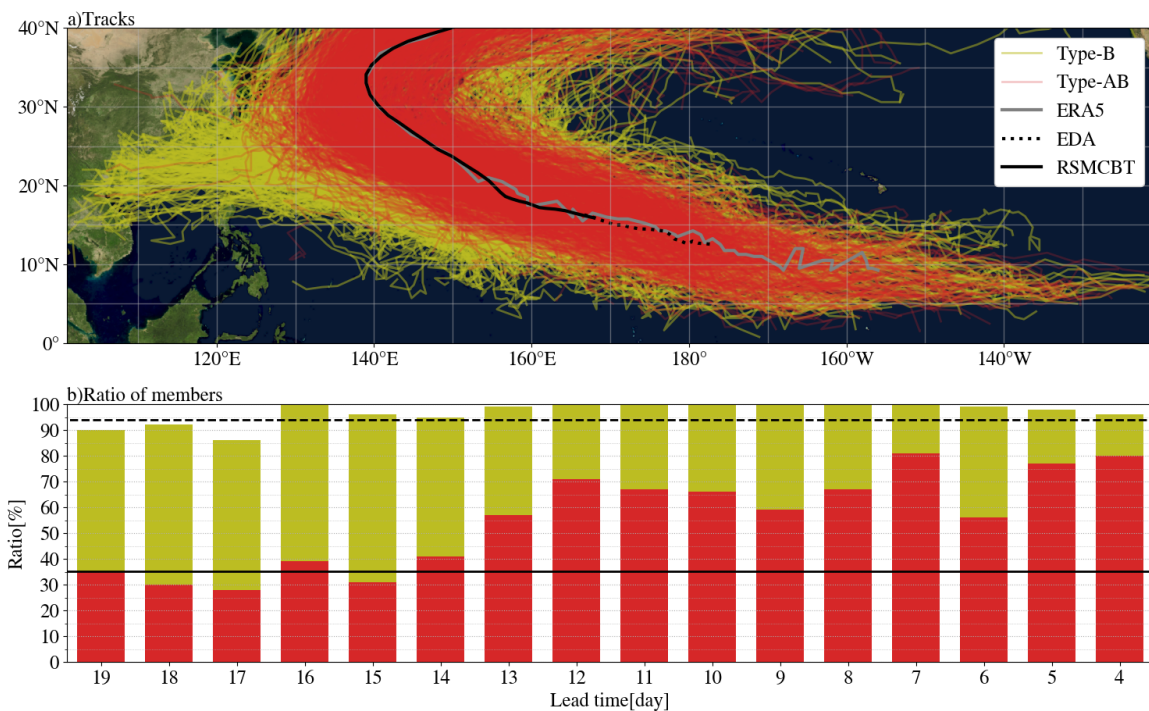
155 The same method as in the ensemble experiment was used for extracting Faxai's vortices from
 156 ERA5. Pre-Faxai in ERA5 could be detected as far back as 06 UTC on August 24, 2019 (Fig. 1a)

157 The results of the ensemble simulations with the 1.25° horizontal resolution regridded from
 158 the original resolution were used to analyze the atmospheric environments of TCs.

159

160 3 Results

161



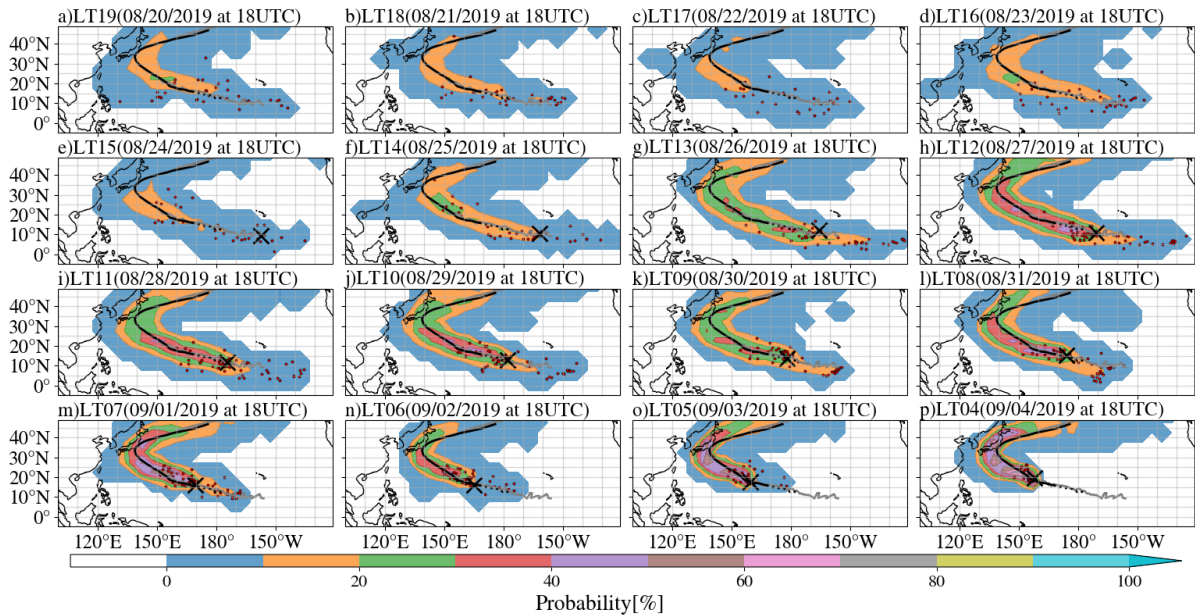
162

163 Figure 1. (a) Plan view of simulated tracks of Faxai-like vortices in a 1600-member Faxai ensemble
 164 simulation. The red and yellow lines denote the tracks of type-AB and type-B vortices,
 165 respectively. The black solid, black dashed, and solid gray lines denote the RSMCBT, EDA, and
 166 ERA5, respectively. Topography and bathymetry are Blue Marble: Next generation (September)
 167 which was produced by Reto Stöckli, NASA Earth Observatory. (b) Ratio of ensemble members
 168 reproducing Faxai-like vortices to respective 100 members for each LT. The red and yellow bars
 169 indicate the rates of those reproducing type-AB and type-B vortices, respectively, for each LT.
 170 The solid and dashed lines denote the mean rate of the ensemble members reproducing type-AB
 171 and type-B vortices, respectively, in NICAM climatology ensemble simulation.

172

173 First, we show tracks of Faxai-like vortices extracted from the 1600 Faxai's ensemble
174 simulation (Fig. 1a). As expected, type-AB vortex tended to approach Japan, whereas type-B
175 vortex seemed to travel westward, eastward, or took a larger detour before moving northward and
176 then traveled toward Japan. Figure 1b shows the percentages of members with Faxai-like vortices
177 exceeding 85% for all LT and the number of members with type-AB vortex increasing
178 conspicuously from LT15 to LT12, instead of a decrease in members with type-AB vortex for
179 LT06.

180 Next, we compared the Faxai's ensemble simulation results with those of the climatology
181 ensemble simulation to determine whether the number of members with Faxai-like vortices
182 changed due to systematic forecast drifts in the model or the influence of the specific environment
183 in 2019. In the climate ensemble simulations, a Faxai-like vortex was generated in approximately
184 95% of members, and type-AB vortex was formed in 35% of members. In other words, about 37%
185 of Faxai-like vortices moved toward Japan. Overall, the ratio of the number of members with the
186 Faxai-like vortices in the Faxai's ensemble simulations was higher than that in the model
187 climatology after LT16. After LT13, the ratio of the number of members with type-AB vortex was
188 higher than that in the model climatology. From the comparison results, the conspicuous increase
189 in the number of members with type-AB vortex in the Faxai's ensemble simulations was not due
190 to systematic drifts but due to the influence of the specific environment in 2019. In summary,
191 NICAM could predict with high accuracy two weeks before landfall that the vortex was likely to
192 head toward Japan.



193

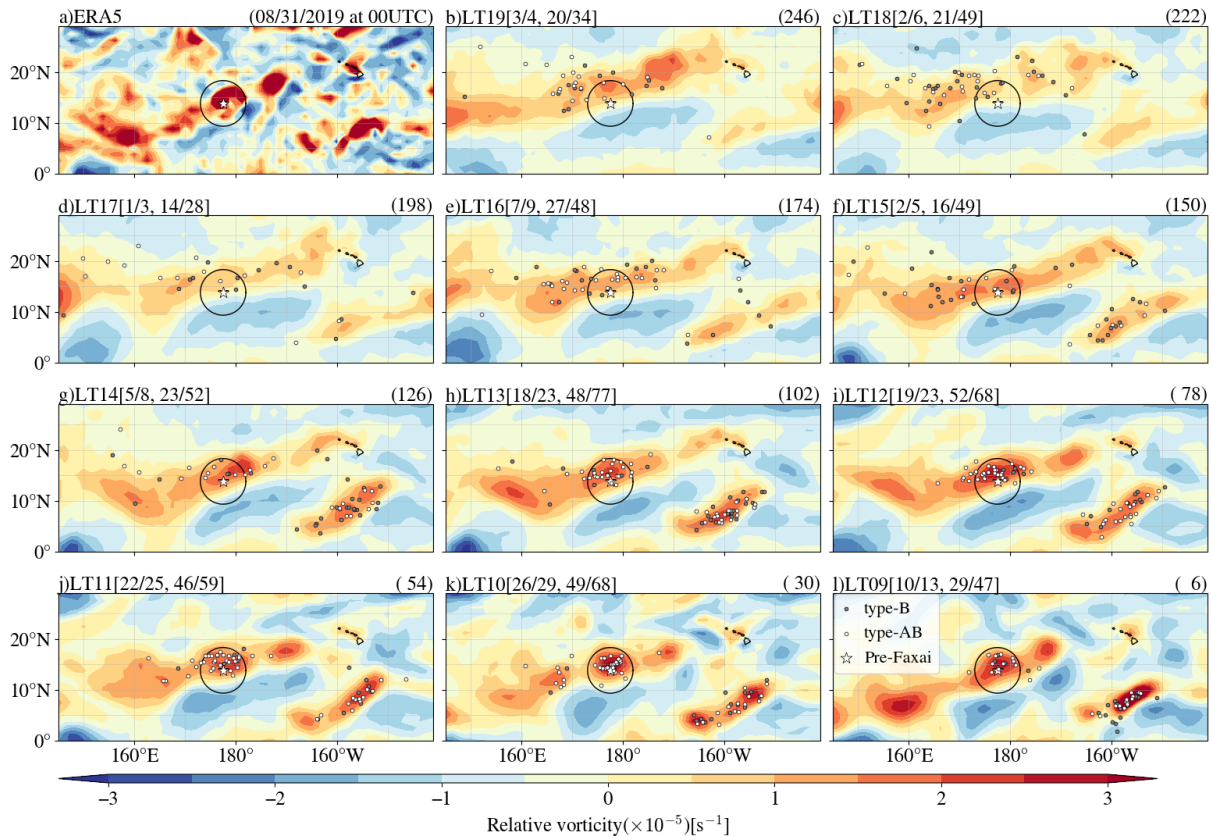
194 Figure 2. Plan views of strike probability density for type-AB vortex for each 100-member
 195 simulation starting from each LT. The density is defined by vortices per 5° cap. The black solid,
 196 black dashed, and solid gray lines denote the RSMCBT, EDA, and ERA5, respectively. The figure
 197 in parentheses indicates the start time of each 100-member ensemble simulation. The cross symbol
 198 indicates the location of Pre-Faxai (e-o) or Faxai (p) at the start time for each LT. These locations
 199 were determined from ERA5. The red circles indicate the starting points of tracks of type-AB
 200 vortex.

201

202 Figure 2 shows the horizontal distribution of strike probability density for type-AB vortex
 203 by each LT (LT19–LT04). For every LT, the strike probability exceeded 10% around the
 204 RSMCBT. From LT15 to LT12, the strike probabilities increased systematically around the
 205 RSMCBT. Although the strike probability in LT11 decreased in the vicinity of east Japan
 206 compared with that in LT12, the strike probability became higher in the vicinity of east Japan with
 207 a shorter LT, indicating that the track of type-AB vortex in the simulation starting from a short LT
 208 became close to the real Faxai track. Figure 2 also shows the starting positions of members with
 209 type-AB vortex. Although the starting positions were sparse for LT19–LT16, they appeared to
 210 become denser along the real Faxai track as the LT became smaller, suggesting that the

211 representation of vorticity was sensitive to LT, which seemed to contribute to the increase in the
 212 number of members with type-AB vortex between LT15 and LT12.

213



214

215 Figure 3. Plan views of the relative vorticity at 850 hPa at 00 UTC on August 31, 2019 for ERA5
 216 (a) and those in the 100-member ensemble mean for LT19 to LT9 (b–l). Numerals in parentheses
 217 on the upper-right side of panels (b–l) indicate forecast time [h]. Positions of type-B and type-AB
 218 vortices at 00 UTC on August 31, 2019, in each LT are embedded on each panel with black and
 219 white circles, respectively. The star-shaped symbol denotes the position of Pre-Faxai analyzed in
 220 the EDA at 00 UTC on August 31. The figures in square brackets indicate the numbers of type-
 221 AB/Faxai-like vortices within the surrounding circle and those in the domain. The number of
 222 Faxai-like vortices is the sum of the numbers of type-B and type-AB vortices.

223

224

225

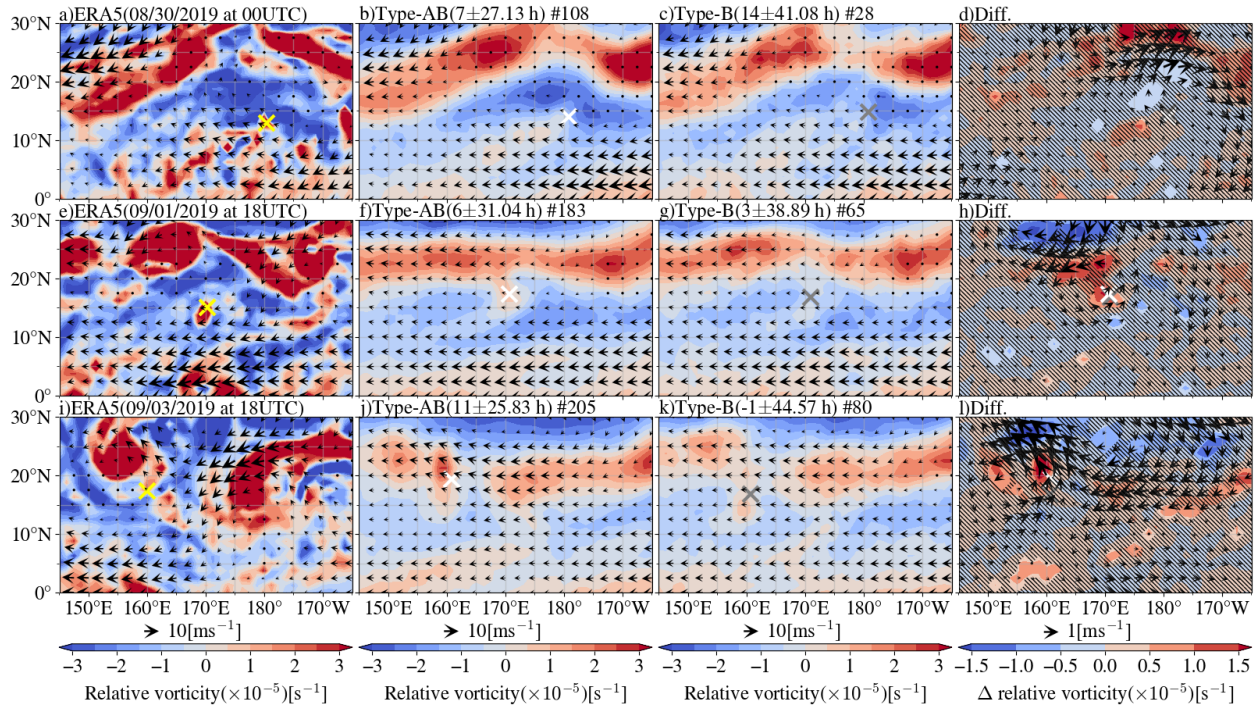
226

227

Figure 3 shows the 100-member ensemble composite of relative vorticity at 850 hPa and
 positions of Faxai-like vortices at 00 UTC on August 31 for LT19–LT09 to investigate why the
 number of members with type-AB vortex increased after LT15. The relative vorticity became
 stronger around Pre-Faxai based on the EDA as the LT became shorter. As for the Faxai-like

228 vortices within a 500-km radius of Pre-Faxai and within the domain, their numbers varied with the
229 LT, which seems to be complicated. The vortices seem to be spontaneously generated in the
230 simulation or included in the initial condition and maintained under favorable environmental
231 conditions. The former may increase over the forecast time, and the latter may increase with the
232 LT becoming shorter. However, the numbers increased rapidly from LT15 to LT12, which were
233 more than four times (from 5 to 23) within a 500-km radius of Pre-Faxai and approximately 1.4
234 times (from 49 to 68) within the domain. This can contribute to the rapid increase in type-AB
235 vortex from LT15 to LT12. In summary, an accurate forecast of a precursor vortex is a key factor
236 for a good forecast of Faxai.

237 With respect to the differences in the tracks between type-AB and type-B vortices,
238 members with type-AB vortex traveled northwestward toward Japan (Fig. 2), whereas most
239 members with type-B vortex traveled westward, took a larger detour before moving northward,
240 and then traveled toward Japan (Supporting Information Fig. S2). Next, we address the reason for
241 differences in tracks between type-AB and type-B vortices. Figure 1a shows that the track of a
242 vortex changed from west–northwest to northwest near 160°E. As the members with type-AB
243 vortex increased after LT15, we composite the members with type-AB and type-B vortices from
244 LT15 to LT08 and compare their synoptic environments before those vortices reached 160°E.
245 Figure 3 shows that the locations of the Faxai-like vortices are roughly divided into two regions:
246 around Pre-Faxai (near 15°N, 178°E) and its southeast side (near 10°N, 155°W). Each vortex
247 seems to be affected by differences in synoptic-scale flow. For ease in comparison between type-
248 AB and type-B vortices, we ignored ensemble members with Faxai-like vortices being the
249 southeast side of Pre-Faxai. We excluded the members whose starting location of the track was 5°
250 east far from the location detected in ERA5 at the same time.



251
 252 Figure 4. Plan views of relative vorticity at a 300-hPa and steering flow when the vortices existed
 253 at 180°: (a) ERA5, (b) type-AB vortex composite, (c) type-B vortex composite, and (d) difference
 254 between type-AB and type-B vortices when the mean longitude of vortices was approximately
 255 180°. (e–h) The same as (a–d), respectively, but for 170°E. (i–l) The same as (a–d), respectively,
 256 but for 160°E. The yellow cross denotes the positions of Pre-Faxai analyzed in the EDA (a and e)
 257 and Faxai analyzed in the RSMCBT (i). The white and gray crosses indicate the ensemble mean
 258 positions of type-AB and type-B vortices, respectively. The hatch indicates regions in which
 259 differences between type-AB and type-B vortices are statistically not significant at 95% with the
 260 Welch t-test. The panels for ERA5 show the date at the top. The panels for type-AB and type-B
 261 vortex composites show the mean time difference from the date of ERA5 with the standard
 262 deviation at the top. The integers on the right side of the sharp mark indicate the numbers of
 263 ensemble members in each composite case.

264
 265 As Fudeyasu et al. (2022) showed the influence of UTCL on Faxai, we focused on the
 266 upper-level vorticity and steering flow. The steering flow was calculated using the formula of
 267 Colbert and Soden (2012) after moving averages were evaluated over a rectangular area of $10^\circ \times$
 268 10° . The upper, middle, and lower panels in Fig. 4 show the horizontal distribution of relative
 269 vorticity at the 300-hPa and steering flow when the vortices existed at 180°, 170°E, and 160°E,
 270 respectively.

271 When the vortex is located around 180° (Figs. 4a–4c), a westward steering flow existed at
272 the south of the vortex. Meanwhile, the steering flow was weak in the north of the vortex. The
273 north of 15°N is a region with the positive vorticity zonally extended with meandering. The
274 positive vorticity region corresponds to the tropical upper-tropospheric trough (TUTT). The
275 difference in the upper-level flows between the type-AB and type-B vortex composites is
276 statistically not significant in most areas around the vortices (Fig. 4d).

277 When the vortex moved further west and reached 170°E (Figs. 4e–4g), the distance from
278 the TUTT to the vortices except for type-B vortex composite reduced. The difference in the relative
279 vorticity between type-AB and type-B vortex composites was significant (Fig. 4h). The difference
280 in the steering flow deflected northeastward, indicating that type-AB vortex tended to travel
281 northward compared with type-B vortex.

282 At the arrival time of the vortex around 160°E , it was confirmed that type-AB vortex had
283 been coupled with the upper-tropospheric vortex (Fig. 4j), the same as in the ERA5 field (Fig. 4i).
284 In addition, a positive vorticity maximum is located just over the west of type-AB vortex;
285 therefore, type-AB vortex can be steered toward northwestward. However, this feature cannot be
286 confirmed for the type-B vortex composite (Fig. 4k); thus, the vortex traveled westward without
287 heading northward. The location of TUTT could have separated the tracks between type-AB and
288 type-B vortices, whether the vortex headed toward Japan (type-AB vortex) or not (type-B vortex).

289

290 **4 Discussions**

291 For precursor vortices that approached Japan (type-AB), their movement tended to be
292 forced by southerly steering flow when they existed from 180° to 160°E (Fig. 4). This southerly
293 steering flow may be induced by a TUTT or cut-off low (Wei et al., 2016). When a TUTT or cut-

294 off low exists on the northwest side of a TC, the vertical wind shear becomes weakened around
295 the TC (Wei et al., 2016). The relatively small vertical wind shear is a favorable environment for
296 TC formation, which agrees with our result that a precursor vortex was more intensified in type-
297 AB ($24.4 \pm 10.5 \text{ ms}^{-1}$) than in type-B ($17.0 \pm 7.0 \text{ ms}^{-1}$) when the vortices arrived at 160°E .
298 However, Fudeyasu et al. (2022) reported that the intensification of Faxai was suppressed by a cut-
299 off low due to an increase in vertical wind shear near the cut-off low. The reason for this
300 inconsistency with our results is unclear. Wei et al. (2016) noted that TC intensification near a cut-
301 off low depends on the relative location and distance because of the interaction between a TC and
302 cut-off low. This is a topic for future work, and it would be possible to quantify the interaction
303 because the high-resolution large ensemble experimental results can be obtained based on our
304 technique.

305 Another discussion is on the origin of type-AB vortex. Figures 3f-l show two clusters of
306 Faxai-like vortices. The first cluster was located around Pre-Faxai, which could be regarded as the
307 correct vortex. The second vortex cluster was located on the southeast side of Pre-Faxai, which
308 could be regarded as another vortex (possible vortex). The possible vortex increased from LT15
309 and decreased from LT08, whereas the correct vortex increased as the LT became shorter
310 (Supporting Information Fig. S3). The compensation between possible and correct vortices can
311 contribute to the decrease in the number of ensemble members with type-AB vortex at LT06 shown
312 in Fig. 1b. Moreover, this result suggests that two kinds of the precursor vortices developed into a
313 typhoon and approached Japan. In Fig. 3, because ERA5 also shows a relatively strong vortex on
314 the southeast side of Pre-Faxai, the possible vortex seems to be not fully unreasonable. TCs that
315 originated from the possible vortex and approached Japan tended to arrive near Japan later and
316 became stronger than those that originated from correct vortices (Supporting Information Figs. S4

317 and S5). The delayed arrival was because the possible vortex tended to travel from farther
318 south–eastward (Fig. 2 and Supporting Information Fig. S2), whereas the long duration over warm
319 water yielded intense TCs, as documented by Camargo and Sobel (2006).

320 **5 Summary and Concluding remarks**

321 A high-resolution large-member ensemble simulation was performed for Typhoon Faxai
322 2019, which caused a severe disaster, particularly in the Tokyo metropolitan area. We found that
323 the risk of Faxai approaching Japan was enhanced two weeks before the landfall in Japan. Detailed
324 data analysis showed that the ensemble simulation covers not only the scenario that Faxai
325 developed from a precursor vortex in the western positively vortical area (near 180° in Fig. 3) as
326 in reality but also a potential scenario in which a similar but a later and stronger TC approaches
327 Japan, formed at a different area far southeast of the real vortex.

328 A reason for the increase in the number of ensemble members with type-AB vortex from
329 two weeks in advance was a rapid increase in the number of members with the precursor vortex
330 from LT15 to LT12. In addition, the TUTT played an essential role in the track simulation of Faxai.
331 The result suggests the accurate simulation of the TUTT and associated cut-off low is crucial for
332 simulating an accurate track of Faxai by improving steering flow.

333

334

335 **Acknowledgments**

336 This research used computational resources of the supercomputer Fugaku by the RIKEN (ID:
337 hp200128, hp210166, hp220167) supported by Ministry of Education, Culture, Sports, Science
338 and Technology (JPMXP1020351142) as “Program for Promoting Researches on the
339 Supercomputer Fugaku” (Large Ensemble Atmospheric and Environmental Prediction for Disaster

340 Prediction and Mitigation). NEXRA used for the initial conditions for 1600-member ensemble
341 simulation is provided by JAXA. The RSMCBT and EDA data are provided by JMA. ERA5 is
342 provided by ECMWF via the Copernicus Climate Change Service Climate Data Store. The authors
343 would like to thank Enago (www.enago.jp) for English language review.

344

345 **Open Research**

346 RSMCBT is available at ([https://www.jma.go.jp/jma/jma-eng/jma-center/rsmc-hp-pub-](https://www.jma.go.jp/jma/jma-eng/jma-center/rsmc-hp-pub-eg/besttrack.html)
347 [eg/besttrack.html](https://www.jma.go.jp/jma/jma-eng/jma-center/rsmc-hp-pub-eg/besttrack.html)); The EDA used in this study is available at Supporting Information Table S1;
348 ERA5 is available at (<https://www.ecmwf.int/en/forecasts/datasets/reanalysis-datasets/era5>); NEXRA
349 is available at (<https://www.eorc.jaxa.jp/theme/NEXRA/guide.htm>); ALERA2 is available at
350 (<https://www.jamstec.go.jp/alera/alera2.html>). NICAM simulation data and vortex tracking code used
351 in this study are available at (Yamada, 2022, <https://zenodo.org/record/6889432>). The model source
352 code is shared with the NICAM community and available at (Kodama et al., 2020,
353 <https://zenodo.org/record/3727329>) as long as the user follows the terms and condition on
354 (<http://nicam.jp/hiki/?Research+Collaborations>). Figures were plotted by using Matplotlib
355 (<https://matplotlib.org/stable/index.html>), Cartopy (Met Office, 2022,
356 <https://zenodo.org/record/6775197>), MetPy (May et al., 2022,
357 <https://www.unidata.ucar.edu/software/metpy/>), and SciPy (Virtanen et al., 2020, <https://scipy.org/>).

358

359

360 **References**

361 Camargo, S. J., & Sobel, A. H. (2005), Western North Pacific tropical cyclone intensity and
362 ENSO. *Journal of Climate*, 18(15), 2996–3006. doi:10.1175/JCLI3457.1

363

- 364 Chan, J. C. L. (2017). Physical mechanisms responsible for track changes and rainfall
365 distributions associated with tropical cyclone landfall. Oxford Handbooks Online,
366 doi:10.1093/oxfordhb/9780190699420.013.16
367
- 368 Colbert, A. J., & Soden, B. J. (2012), Climatological variation in North Atlantic tropical cyclone
369 tracks, *Journal of Climate*, 25(2), 657–673. doi:10.1175/JCLI-D-11-00034.1
370
- 371 Enomoto, T., Miyoshi, T., Moteki, Q., Inoue, J., Hattori, M., Kuwano–Yoshida, A., Komori, N.,
372 & Yamane, S. (2013). Observing-system research and ensemble data assimilation at JAMSTEC.
373 In: Park, S., Xu, L. (Eds.), *Data Assimilation for Atmospheric, Oceanic and Hydrologic*
374 *Applications* (Vol. 2, pp. 509–526). Berlin, Heidelberg: Springer. doi:10.1007/978-3-642-35088-
375 7_21
376
- 377 Fudeyasu, H., Shimada, U., Oikawa, Y., Eito, H., Wada, A., Yoshida, R., & Horinouchi, T.
378 (2022). Contributions of the large-scale environment to the typhoon genesis of Faxai (2019).
379 *Journal of the Meteorological Society of Japan*, 100(4). doi:10.2151/jmsj.2022-031
380
- 381 Hersbach, H., Bell, B., Berrisford, P., Hirahara, S., et al. (2020). The ERA5 global reanalysis.
382 *Quarterly Journal of the Royal Meteorological Society*, 146(730), 1999–2049.
383 doi:10.1002/qj.3803
384

385 Huang, B., Liu, C., Banzon, V., Freeman, E., Graham, G., Hankins, B., Smith, T., & Zhang, H.-
386 M. (2021). Improvements of the Daily Optimum Interpolation Sea Surface Temperature
387 (DOISST) Version 2.1. *Journal of Climate*, 34(8), 2923–2939. doi:10.1175/JCLI-D-20-0166.1

388

389 Ito, K., Wu, C.-C., Chan, K. T. F., Toumi, R., & Davis, C. (2020). Recent progress in the
390 fundamental understanding of tropical cyclone motion. *Journal of the Meteorological Society of*
391 *Japan. Ser. II*, 98(1), 5–17. doi:10.2151/jmsj.2020-001

392

393 Japan Meteorological Agency (JMA). (2020). Annual Report on the Activities of the RSMC
394 Tokyo–Typhoon Center 2019. Retrieved from [https://www.jma.go.jp/jma/jma-eng/jma-](https://www.jma.go.jp/jma/jma-eng/jma-center/rsmc-hp-pub-eg/AnnualReport/2019/Text/Text2019.pdf)
395 [center/rsmc-hp-pub-eg/AnnualReport/2019/Text/Text2019.pdf](https://www.jma.go.jp/jma/jma-eng/jma-center/rsmc-hp-pub-eg/AnnualReport/2019/Text/Text2019.pdf)

396

397 Kinter, J. L., III, Cash, B., Achuthavarier, D., Adams, J., Altshuler, E., Dirmeyer, P., et al.
398 (2013). Revolutionizing climate modeling with Project Athena: A multi-institutional,
399 international collaboration. *Bulletin of American Meteorological Society*, 94(2), 231–245.
400 doi:10.1175/BAMS-D-11-00043.1

401

402 Kishimoto, K. (2009). Revision of JMA’s early stage Dvorak analysis and its use to analyze
403 tropical cyclones in the early developing stage (Technical Review, No. 10). Tokyo, Japan:
404 RSMC Tokyo–Typhoon Center. Retrieved from [https://www.jma.go.jp/jma/jma-eng/jma-](https://www.jma.go.jp/jma/jma-eng/jma-center/rsmc-hp-pub-eg/techrev/text10-1.pdf)
405 [center/rsmc-hp-pub-eg/techrev/text10-1.pdf](https://www.jma.go.jp/jma/jma-eng/jma-center/rsmc-hp-pub-eg/techrev/text10-1.pdf)

406

407 Kodama, C., Ohno, T., Seiki, T., Yashiro, H., Noda, A. T., Nakano, M., et al. (2021). The
408 Nonhydrostatic ICosahedral Atmospheric Model for CMIP6 HighResMIP simulations
409 (NICAM16-S): experimental design, model description, and impacts of model updates,
410 *Geoscientific Model Development*, 14(2), 795–820. doi:10.5194/gmd-14-795-2021
411

412 Kodama, C., Ohno, T., Seiki, T., Yashiro, H., Noda, A. T., Nakano, M., et al. (2020). The
413 Nonhydrostatic ICosahedral Atmospheric Model for CMIP6 HighResMIP simulations
414 (NICAM16-S) [Software]. Zenodo. <https://zenodo.org/record/3727329>
415

416 Kotsuki, S., Terasaki, K., Kanemaru, K., Satoh, M., Kubota, T., & Miyoshi, T., (2019).
417 Predictability of record-breaking rainfall in Japan in July 2018: Ensemble forecast experiments
418 with the near-real-time global atmospheric data assimilation system NEXRA. *Scientific Online*
419 *Letters on the Atmosphere*, 15, 1–7. doi:10.2151/sola.15A-001
420

421 Magnusson, L., Doyle, J. D., Komaromi, W. A., Torn, R. D., Tang, C. K., Chan, J. C. L.,
422 Yamaguchi, M., & Zhang, F. (2019). Advances in understanding difficult cases of tropical
423 cyclone track forecasts. *Tropical Cyclone Research and Review*, 8(2), 109–122.
424 doi:10.1016/j.tcr.2019.10.001
425

426 May, R. Arms, M., Marsh, S. C., Bruning, P., Leeman, E., Goebbert, J. R., et al. (2022). MetPy:
427 A Python Package for Meteorological Data version 1.3.0 [Software]. Unidata,
428 <https://doi.org/10.5065/D6WW7G29>
429

430 Met Office. (2022). SciTools/cartopy: v0.20.3 [Software]. Zenodo.

431 <https://doi.org/10.5281/zenodo.1182735>

432

433 Miyamoto, Y., Fudeyasu, H., & Wada, A. (2022). Intensity and structural change of numerically
434 simulated Typhoon Faxai (1915) before landfall. *Journal of the Meteorological Society of Japan*,
435 *Ser. II*, 100(1), 181–196. doi:10.2151/jmsj.2022-009

436

437 Nakano, M., Sawada, M., Nasuno, T., & Satoh, M. (2015), Intraseasonal variability and tropical
438 cyclogenesis in the western North Pacific simulated by a global nonhydrostatic atmospheric
439 model. *Geophysical Research Letters*, 42(2), 565–571. doi:10.1002/2014GL062479

440

441 Nakano, M., Wada, A., Sawada, M., et al. (2017). Global 7-km mesh nonhydrostatic model
442 intercomparison project for improving typhoon forecast (TYMIP-G7): Experimental design and
443 preliminary results. *Geoscientific Model Development*, 10(3), 1363–1381. doi:10.5194/gmd-10-
444 1363-2017

445

446 Nakano, M., Chen, Y.-W., & Satoh, M. (2022). Analysis of the factors that led to an uncertainty
447 of track forecast of Typhoon Krosa (2019) by 101-member ensemble forecast experiments using
448 NICAM. *Jxiv*. doi:10.51094/jxiv.46

449

450 Roberts, M. J., Camp, J., Seddon, J., Vidale, P. L., Hodges, K., Vannière, B., et al. (2020).

451 Projected future changes in tropical cyclones using the CMIP6 HighResMIP multimodel

452 ensemble. *Geophysical Research Letters*, 47(14), e2020GL088662. doi:10.1029/2020GL088662

453

- 454 Satoh, M., Matsuno, T., Tomita, H., Miura, H., Nasuno, T., & Iga, S. (2008) Nonhydrostatic
455 icosahedral atmospheric model (NICAM) for global cloud resolving simulations. *Journal of the*
456 *Computational Physics*, 227(7), 3486–3514. doi:10.1016/j.jcp.2007.02.006
457
- 458 Satoh, M., Tomita, H., Yashiro, H., Miura, H., Kodama, C., Seiki, T., et al. (2014). The non-
459 hydrostatic icosahedral atmospheric model: Description and development. *Progress in Earth and*
460 *Planetary Science*, 1(1), 18. doi:10.1186/s40645-014-0018-1
461
- 462 Tomita, H., & Satoh, M. (2004). A new dynamical framework of nonhydrostatic global model
463 using the icosahedral grid. *Fluid Dynamics Research*, 34(6), 357–400.
464 doi:10.1016/j.fluidyn.2004.03.003
465
- 466 Virtanen, P., Gommers, R., Oliphant, T. E., Haberland, M., Reddy, T., Cournapeau, D., et al.,
467 (2020) SciPy 1.0: Fundamental Algorithms for Scientific Computing in Python. *Nature Methods*,
468 17(3), 261–272. Doi:10.1038/s41592-019-0686-2
469
- 470 Vitrat, F. (2014). Evolution of ECMWF sub-seasonal forecast skill scores. *Quarterly Journal of*
471 *the Royal Meteorological Society*, 140(683), 1889–1899. doi:10.1002/qj.2256
472
- 473 Wada, A., Yanase, W., & Okamoto, K. (2022). Interactions between a tropical cyclone and
474 upper-tropospheric cold-core lows simulated by an atmosphere-wave-ocean coupled model: A
475 case study of Typhoon Jongdari (2018). *Journal of the Meteorological Society of Japan. Ser. II*,
476 100(2), 387–414. doi:10.2151/jmsj.2022-019

477

478 Wei, N., Li, Y., Zhang, D., Mai, Z., & Yang, S. (2016). A statistical analysis of the relationship
479 between upper-tropospheric cold low and tropical cyclone track and intensity change over the
480 western North Pacific. *Monthly Weather Review*, *144*(5), 1805–1822, doi:10.1175/MWR-D-15-
481 0370.1

482

483 Yamada, H., Nasuno, T., Yanase, W., & Satoh, M. (2016). Role of the vertical structure of a
484 simulated tropical cyclone in its motion: a case study of typhoon Fengshen (2008). *Scientific
485 Online Letters on the Atmosphere*, *12*, 203–208, doi:10.2151/sola.2016-041

486

487 Yamada, Y. (2022). Data used in a manuscript entitled "Large ensemble simulation for
488 investigating predictability of precursor vortices of Typhoon Faxai in 2019 with a 14-km mesh
489 global nonhydrostatic atmospheric model" submitted to *Geophysical Research Letters* [Dataset].
490 Zenodo. <https://doi.org/10.5281/zenodo.6889432>

491

492 Yamaguchi, M., Ishida, J., Sato, H., & Nakagawa, M. (2017). WGNE intercomparison of
493 tropical cyclone forecasts by operational NWP models: A quarter century and beyond. *Bulletin of
494 the American Meteorological Society*, *98*(11), 2337–2349. doi:10.1175/BAMS-D-16-0133.1

495

496